Impact of the Generation and Activation of Sea Salt Aerosols on the Evolution of Tropical Cyclone Dumile

Thomas Hoarau, Christelle Barthe, Pierre Tulet, Marine Claeys, Jean-Pierre Pinty, Olivier Bousquet, Julien Delanoë, Benoit Vié

Journal of Geophysical Research: Atmospheres

RESEARCH ARTICLE
10.1029/2017JD028125

Impact of the Generation and Activation of Sea Salt Aerosols on the Evolution of Tropical Cyclone Dumile

T. Hoarau[1], C. Barthe[1], P. Tulet[1], M. Claeys[1], J.-P. Pinty[2], O. Bousquet[1], J. Delanoë[3], and B. Vié[4]

[1]Laboratoire de l'Atmosphère et des Cyclones, UMR 8105 CNRS/Météo-France/Université de La Réunion, Saint Denis, France, [2]Laboratoire d'Aérologie, UMR 5560 CNRS/Université de Toulouse, Toulouse, France, [3]LATMOS/IPSL/UVSQ/CNRS, Guyancourt, France, [4]Centre National de Recherches Météorologiques, UMR 3589 Météo-France/CNRS, Toulouse, France

Key Points:
- The coupling between an aerosol scheme and a two-moment microphysics scheme is done in the cloud-resolving model Meso-NH
- Explicitly taking account of sea salt aerosol emissions associated with high winds and waves in tropical cyclones is essential

Correspondence to:
C. Barthe,
christelle.barthe@univ-reunion.fr

Citation:
Hoarau, T., Barthe, C., Tulet, P., Claeys, M., Pinty, J.-P., Bousquet, O., et al. (2018). Impact of the generation and activation of sea salt aerosols on the evolution of tropical cyclone Dumile. *Journal of Geophysical Research: Atmospheres*, *123*, 8813–8831. https://doi.org/10.1029/2017JD028125

Received 28 NOV 2017
Accepted 18 JUL 2018
Accepted article online 25 JUL 2018
Published online 24 AUG 2018

Abstract An original coupling between an aerosol scheme and a two-moment microphysics scheme has been developed in the cloud-resolving model Meso-NH to fully represent the aerosol-microphysics-dynamics interactions in tropical cyclones. A first evaluation of this coupling is performed through the simulation of tropical cyclone Dumile (2013) in the South-West Indian Ocean. MACC (Monitoring Atmospheric Composition and Climate project) analysis and CALIPSO (Cloud-Aerosol Lidar and Infrared Pathfinder Satellite Observations) data agree about the predominance of sea salt aerosols. The aerosol-microphysics coupled system reproduces the track and intensity of Dumile well, with a transition from a monsoon depression to a tropical cyclone, and produces ice water contents that compare well with the DARDAR (raDAR/liDAR) product. Using a one-moment microphysics scheme produces a more intense and symmetric system tracking too far to the west. In the aerosol-microphysics coupled simulation, sea salt aerosols, the main source of cloud condensation nuclei (CCN), are preferentially produced in regions with high winds and waves, which reinforce convective asymmetries compared to the simulation with the one-moment scheme. Using a two-moment microphysics scheme without explicit sea salt emission led to a dramatic weakening of Dumile after 24 hr of simulation due to the consumption and scavenging of all interstitial CCN in the inner core. The importance of explicitly taking account of sea salt aerosol emissions associated with high winds and waves in tropical cyclones is a critical point for simulating long-lasting systems that need to generate their own CCN.

1. Introduction

The main issue for tropical cyclone forecasters is to predict the track, the intensity, and the hazards associated with the passage of storms close to inhabited regions. Track forecasting has been improved recently thanks to model developments, higher grid resolutions, and data assimilation to better represent large-scale flows. However, forecasting the intensity and the hazards (wind, precipitation, and marine surge) associated with tropical storms remains a major issue for the scientific community. The lack of observations over the oceans, the models' limitations in terms of physical parameterizations and resolution, and the lack of knowledge of some physical processes involved in tropical cyclone intensification remain a scientific challenge.

The evolution of tropical cyclone intensity is determined by multiscale factors such as the synoptic environment, inner-core dynamics, and ocean surface conditions. Among these factors, the key role of microphysics has been highlighted. Willoughby et al. (1984) and Lord et al. (1984) first showed the importance of ice microphysics in the development and structure of a modeled hurricane vortex. The cooling effect associated with the melting of ice particles was shown to modify the mesoscale vertical velocity structures of the storm. Thereafter, numerous studies investigated the impact of microphysics on the intensity, structure, and development of tropical cyclones in detail.

Microphysical processes have been shown to greatly impact the structure and intensity of a simulated storm. In particular, evaporation of cloud droplets and raindrops has been pointed out as key processes for the system intensification and structure (Li et al., 2013a; Wang, 2002; Zhu & Zhang, 2006) through the formation of downdrafts and rainbands. Through the computation of budgets in Typhoon Hagupit (2008), Li et al. (2013b) concluded that the typhoon intensity could be enhanced through latent heat release associated with condensation and deposition growth of cloud ice and snow, while the latent heat absorption associated with sublimation of snow, melting of graupel, and evaporation of rain tended to weaken the intensity. The choice of the dimensional parameters of the hydrometeors is also of great importance for tropical cyclone modeling. In particular, the graupel fall speed has a direct effect on modeled low-level winds and central pressure

(McFarquhar et al., 2006; McFarquhar & Black, 2004), precipitation structures (Franklin et al., 2005), and lightning activity (Barthe et al., 2016).

As a result, using different microphysics schemes can impact the tropical cyclone structure and intensity (Li & Pu, 2008). Recently, several studies have attempted to evaluate the impact of using a multimoment microphysics scheme. Using WRF-ARW (Weather Research and Forecasting-Advance Research WRF), Islam et al. (2015) investigated the best set of physical parameterizations to reproduce the track and intensity of Supertyphoon Haiyan (2013). While the track of the system was fairly well reproduced by all the combinations of physical parameterizations, the intensity was systematically underestimated. This may have been due to a strong underestimation of the intensity (~55 hPa for the minimum sea level pressure, MSLP) in the initial state. The use of the Milbrandt and Yau's (2005) double-moment microphysics scheme did not change the results in terms of intensity. Jin et al. (2014) compared the impact of single- and double-moment microphysics schemes on the prediction of a tropical cyclone environment in the COAMPS-TC model. The single-moment microphysics scheme based on Rutledge and Hobbs's work (Rutledge & Hobbs, 1983) produced an excess of upper-level cloud ice. The hybrid two-moment scheme of Thompson et al. (2008), which treats rain and cloud ice with two moments and cloud water, snow, and graupel with one moment, led to a reduction of 2 orders of magnitude in the upper-level cloud ice produced by the single-moment scheme. This reduction of upper-level cloud ice was attributed to differences of ice nucleation parameterization. The Fletcher (1962) formulation used in the one-moment scheme tended to produce much higher ice concentrations at cold temperatures than the Cooper (1986) formulation did in the two-moment scheme. This excess of cloud ice in the upper levels resulted in an upper-level warm bias associated with the longwave radiative heating at the base of the ice layer. The extension of the 500-hPa subtropical high that controls the tropical cyclone tracks was also affected. Consequently, the two-moment scheme helps to reduce the track errors and the occurrence of over intensification of storms. However, in these studies, the differences in tropical cyclone behavior could not be attributed to the number of moments of the microphysics schemes but rather to differences in the representation of some microphysical processes.

More sophisticated microphysical schemes are being developed in cloud resolving models. Recent schemes treat the effects of aerosol particles in a more realistic and exhaustive manner. Using a multimoment or a bin microphysical scheme generally requires cloud condensation nuclei (CCN) and ice freezing nuclei (IFN) concentrations to predict the cloud water and cloud ice number concentrations, and studies about the effect of aerosols on clouds in tropical cyclones are thus now possible. In particular, it has been shown that increasing the CCN number concentration at the periphery of the tropical cyclone tends to decrease its intensity (Carrio & Cotton, 2011; Hazra et al., 2013; Khain et al., 2008, 2010; Wang et al., 2014; Zhang et al., 2007). As hypothesized by Rosenfeld et al. (2012), dust or pollution aerosols in the vicinity of the outer rainbands act as CCN and increase the number of cloud droplets while decreasing their size, thus delaying the formation of rain (Albrecht, 1989; Twomey, 1977) and increasing the formation of ice particles aloft (Carrio & Cotton, 2011; Van den Heever et al., 2006; Van den Heever & Cotton, 2007). The convection invigoration of the rainbands associated with this additional latent heat release during liquid water freezing would reduce the low-level convergence of moist air toward the inner core of the system, lowering the maximum wind speed. This effect would be amplified by the cooling of the converging low-level air due to the melting and evaporation of the enhanced ice content. However, using the Regional Atmospheric Modeling System with two-moment bin-emulating bulk microphysics (Saleeby & Cotton, 2008), Herbener et al. (2014) showed that the tropical cyclone had a reduced size and was more intense when a source of aerosol particles was located at the periphery of the storm. The penetration of aerosol particles into the inner core of the system and the invigoration of convection in the eyewall can explain the contradictory results. Lynn et al. (2016) performed several simulations of Hurricane Irene (2011) with the WRF model including a spectral bin microphysics scheme (Khain et al., 2010) and variable aerosol spatial distributions. Using a uniform spatial aerosol distribution typical of a maritime environment did not allow the evolution of Irene's intensity to be reproduced. When continental aerosols were specified over land in addition to a 3-km-deep Saharan dust band and maritime aerosols over the sea, an eyewall replacement cycle was reproduced along with the observed 40-hr delay between the minimum pressure and the maximum wind speed. The concentration of cloud droplets increased in the presence of continental aerosols and invigorated the convection in the outer rainbands to form a secondary eyewall. Khain et al. (2016) also tested a large set of microphysical schemes within WRF to investigate the impact of aerosols from the continental United States and the Saharan Air Layer on the development of Irene (2011).

In agreement with previous studies, they showed a strong impact of the choice of the microphysics scheme on the microphysical structure of clouds, the latent heat release profile, and the storm intensity.

However, the impact of the microphysics on the cyclone track is less recognized (Fovell et al., 2010, 2016). Fovell and Su (2007) concluded that the microphysics may impact the tropical cyclone track through the modification of such characteristics as its size and depth, and the radial structure or azimuthal asymmetry, which are known to control the vortex track. As described by Fovell et al. (2009), the assumptions in microphysics tend to modulate the temperature gradients. They largely influence the pressure gradients that indirectly control the track of the system.

Although several studies highlighted the important role of aerosols on the intensity, evolution, structure, or trajectory of tropical cyclones, most of them did not consider all the processes linked to aerosol lifecycle, such as emission, scavenging, or aerosol-radiation interactions. Furthermore, most of the schemes assumed a constant and spatially homogeneous concentration of a single-mode aerosol population as stated by Vié et al. (2016). In particular, tropical cyclones generate their own CCN via sea salt emission under high wind conditions and strong breaking waves. In this context, the objective of this article is to show the importance of an explicit treatment of aerosols when studying tropical cyclones using high-resolution simulations performed with the nonhydrostatic model Meso-NH. The case of tropical cyclone Dumile, which evolved in the South-West Indian Ocean in 2013, is presented in section 2. The coupling between an aerosol scheme (ORILAM, Organic Inorganic Log-normal Aerosol Model; Tulet et al., 2005) and a two-moment microphysical scheme (LIMA, Liquid Ice Multiple Aerosols; Vié et al., 2016) in the Meso-NH model is described in section 3. The numerical setup is presented in section 4. Sections 5 and 6 present the results.

2. The Case Study: Tropical Cyclone Dumile (2013)

The best-track of tropical cyclone Dumile is shown in Figure 1a. The classification used hereafter is that of the Regional Specialized Meteorological Center (RSMC)—Tropical Cyclone at La Réunion. It is based on an estimation of the 10-min averaged maximum surface wind speed.

Dumile started developing from a pulse of the Madden-Julian Oscillation in the South-West Indian Ocean at the end of December 2012. On 27 and 28 December, the synoptic conditions were not favorable as strong wind shear prevented the disturbance from developing while moving west-southwestward. On 29 December, the low level environment improved, with a strengthening of the monsoon flow resulting in a better convergence with the trade winds. However, a strong vertical wind shear was still present over the region. On 30 and 31 December, the center of the system was located near Agalega Island. The circulation was far more extended and disorganized than for a typical cyclonic circulation even though the convective activity was intense. This particular structure looked like a monsoon depression with a large extension of weak winds, the strongest winds being pushed away from the clockwise circulation (Baray et al., 2010; Figure 1b). On 1 January 2013, the track turned toward the south as the steering flow changed due to the development of a midtropospheric ridge located on the eastern side of the system. As the system came closer to the axis of the altitude ridge, the vertical wind shear decreased and Dumile finally adopted a typical tropical storm structure. On 2 January, the inner core of the system contracted and the convective activity developed around the center. The intensity of Dumile continued to increase, reaching the stage of strong tropical storm. During the afternoon of 2 January an eye became visible (Figure 1c). On 3 January, Dumile reached the stage of tropical cyclone as its center passed 105 km west of La Réunion (Figure 1d). On 4 January, a northwest wind shear appeared and the oceanic energy content decreased, leading to a rapid weakening of Dumile while south of the island.

Because it was compact and had a relatively high displacement speed, the eyewall of Dumile only brushed past the island, so severe material damage and human casualties were avoided. Winds affected the island unequally: while the maximum wind gusts peaked at 180 km/hr on mountainous areas, inhabited coasts were impacted by wind gusts of about 100 km/hr or less. Significant wave height of 6.3 m was measured to the northwest of the island. Precipitation during Dumile was mainly associated with orographic effects. The maximum cumulated rainfall on the Piton de la Fournaise volcano reached 1,189 mm (762 mm in 12 hr), while less than 100 mm was reported over coastal areas.

The rest of this study will focus on the period from 1 to 3 January when the cyclone was intensifying and moving southward.

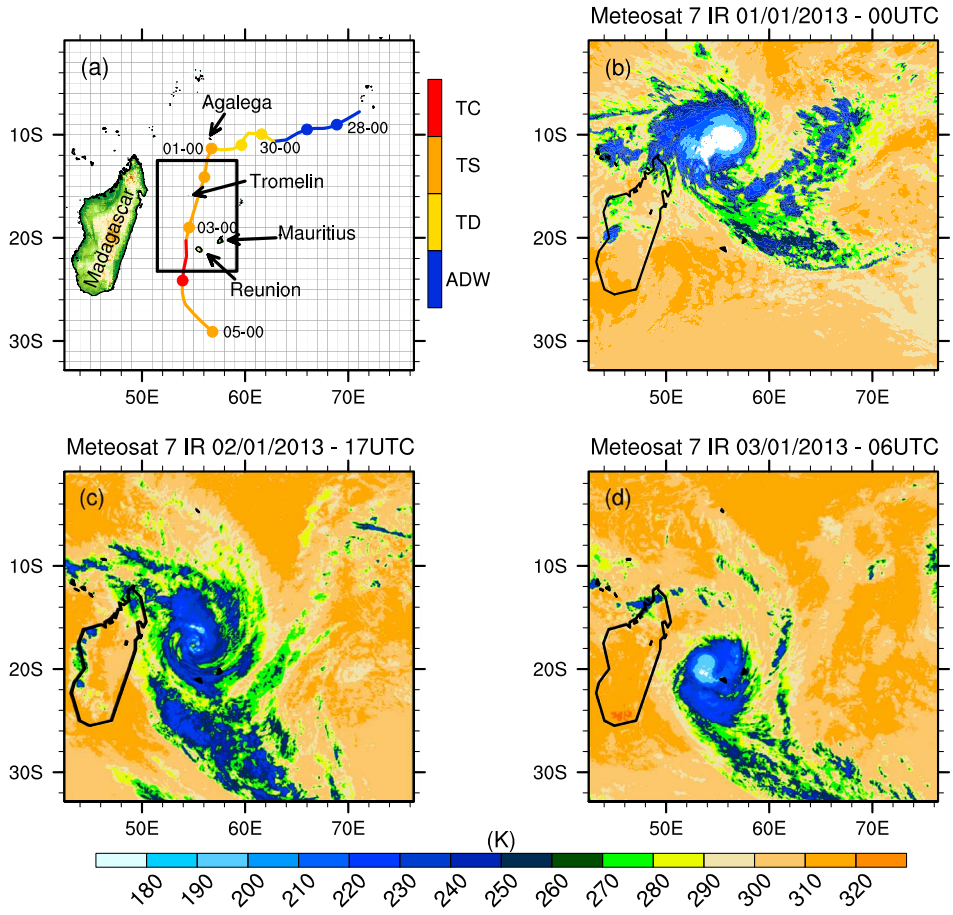

Figure 1. (a) Best-track of Dumile analyzed by RSMC La Réunion (colored line and dots). Four distinct stages are shown: Area of disturbed weather (ADW) in blue, tropical disturbance and tropical or posttropical depression (TD) in yellow, tropical storm (TS) in orange, and tropical cyclone (TC) in red. The outer domain of Meso-NH (D1) covers this whole area while the black box indicates the limits of the inner domain (D2). IR brightness temperature (K) from Meteosat 7 on (b) 1 January 2013 at 00 UTC, (c) 2 January at 17 UTC, and (d) 3 January at 06 UTC.

3. Aerosol-Microphysics Coupling in Meso-NH

The French nonhydrostatic mesoscale atmospheric model Meso-NH (http://mesonh.aero.obs-mip.fr) was used in this study. The coupling between the ORILAM lognormal aerosols scheme and the LIMA two-moment bulk microphysics scheme is detailed below.

3.1. The LIMA Microphysics Scheme

The two-moment microphysics scheme LIMA (Vié et al., 2016) is based on the one-moment microphysics scheme ICE3 (Pinty & Jabouille, 1998). The schemes treat the evolution of the mixing ratio for six water species (water vapor, cloud droplets, raindrops, cloud ice, snow/aggregates, and graupel). Additionally, LIMA predicts the concentration of cloud droplets, raindrops, and cloud ice.

In addition, LIMA handles the competition between several types of aerosols. These modes are characterized by their chemical composition and their hygroscopic capability to act as CCN, IFN, or coated IFN. Two modes of aerosols acting as CCN (sea salt and sulfates), a single mode of aerosols acting as coated IFN (hydrophilic black carbon and organic matter), and two modes of aerosols acting as pure IFN (dust and hydrophobic organic matter and black carbon) are considered. Two prognostic variables are associated with each type of aerosol particle: the number concentration of interstitial aerosols and the number concentration of activated/nucleated aerosols. Their size distribution follows a lognormal size distribution with fixed modal diameter and width.

The CCN activation is parameterized following Cohard et al. (1998) but was extended to handle the competition between several modes of CCN (Vié et al., 2016). The number of activated CCN is computed from an extension of the law given by Twomey (1959). The maximum supersaturation is computed from the convective updraft, the growth of droplets by water vapor condensation, and a cooling rate. The IFN heterogeneous nucleation is parameterized according to Phillips et al. (2008, 2013). In this empirical parameterization, the number of nucleated IFN depends on the nucleating efficiency and on the total surface area, larger particles having more nucleation sites, and so a higher nucleation probability. The specific coated IFN mode serves first as CCN to generated tagged cloud droplets that are subject to ice nucleation by immersion at colder temperature. Homogeneous freezing of cloud droplets is also taken into account and follows Pruppacher (1995), while homogeneous freezing of interstitial CCN follows Kärcher and Lohmann (2002). Secondary ice production by the Hallett-Mossop process (Hallett & Mossop, 1974) is included. In-cloud and below-cloud scavenging of aerosol particles follow Berthet et al. (2010).

3.2. The ORILAM Aerosol Scheme

ORILAM is a three-moment lognormal aerosol scheme (Tulet et al., 2005). Each mode of the size distribution is described by up to three moments (0th, 3rd, and 6th moment). ORILAM handles the sources, emission, transport, dry and wet deposition, and chemistry of aerosols. Since the South-West Indian Ocean has a clean aerosol environment outside the biomass burning season (Duflot et al., 2011), only aerosols of natural origin were considered in the aerosol scheme of this study.

Production of both sea salt and dust aerosols depends on the wind speed. Dust aerosols are simulated using the Dust Entrainment And Deposition (DEAD) model (Zender et al., 2003) developed by Mohktari et al. (2012), in which they are distributed following three lognormal modes (Grini et al., 2006; Tulet et al., 2008). The sea salt aerosols source function from Ovadnevaite et al. (2014) has been recently implemented in Meso-NH (Claeys, 2016). Only the inorganic fraction is considered in this study. Their emission depends not only on the 10-m wind speed but also on the wave height, wind history, friction velocity, and viscosity. Sea salt aerosols are distributed following five lognormal modes. For each mode *i*, the number median radius (r_i, in micron) and the geometric standard deviation (σ_i) are (r_1 = 0.009, σ_1 = 1.37), (r_2 = 0.021, σ_2 = 1.5), (r_3 = 0.045, σ_3 = 1.42), (r_4 = 0.115, σ_4 = 1.53), and (r_5 = 0.415, σ_5 = 1.85). This parameterization covers a large range of diameters from submicron (15 nm) to supermicron particles (6 μm) but does not consider spume drops for which large uncertainties in the generation function remain (Veron, 2015). Once emitted, aerosols are transported by advection and turbulence and can be lost by sedimentation, and dry or wet deposition. In-cloud and below-cloud scavenging of aerosols is parameterized following Tulet et al. (2010). The optical properties of aerosols are computed online as described in Aouizerats et al. (2010): they are deduced from the aerosol chemical composition and the size parameters corresponding to the particles.

3.3. ORILAM-LIMA Coupling

Although LIMA can deal with interstitial and nucleated CCN and IFN (Vié et al., 2016), it was necessary to couple it with an aerosol scheme to handle aerosol emission, transport, and deposition in a coherent way. A coupling between LIMA and the ORILAM aerosol scheme was thus developed: the emission, transport, and wet and dry deposition of sea salt and dust aerosols are treated in the aerosol scheme ORILAM, which are then transferred into LIMA to be used as interstitial CCN and IFN (Figure 2), at each time step. Note that when the coupling between ORILAM and LIMA is activated, sea salt and dust aerosol scavenging is performed only in ORILAM.

The three largest modes of sea salt aerosols in ORILAM are considered as interstitial CCN. These three modes are gathered together in the interstitial CCN variable associated with sea salt aerosols in LIMA. In ORILAM, three modes of dust are available with properties based on those defined in the AMMA (African Monsoon Multidisciplinary Analyses) campaign (Crumeyrolle et al., 2008) in West Africa. The three dust modes in ORILAM are all included in the interstitial IFN mode associated with dust in LIMA.

3.4. ORILAM-LIMA Initialization

As described in Vié and Pinty (2014), the initial and lateral boundary conditions for the aerosols in LIMA can be obtained from the European Center for Medium-Range Weather Forecast (ECMWF) Monitoring Atmospheric Composition and Climate project (MACC; http://www.gmes-atmosphere.eu/). Aerosol

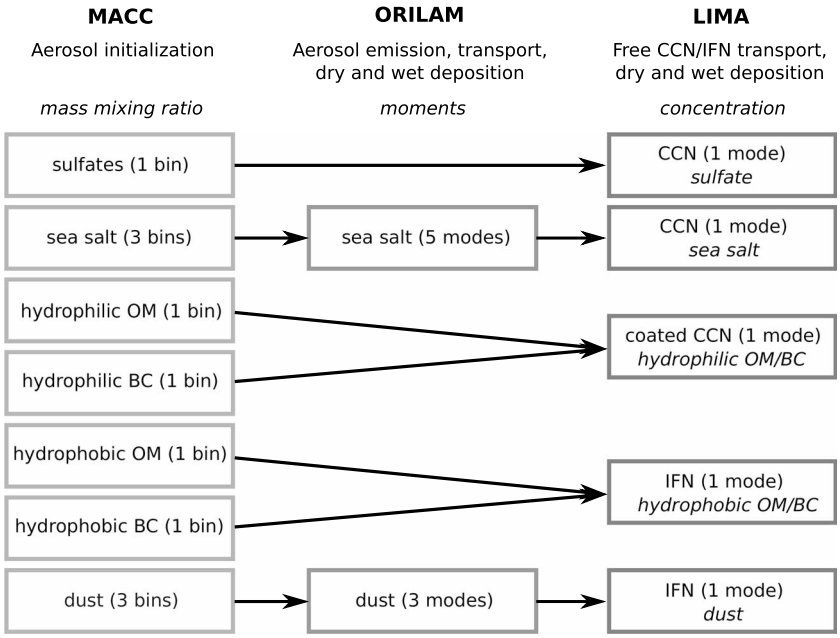

Figure 2. Schematic diagram of the aerosol-microphysics coupling system. OM and BC stand for organic matter and black carbon, respectively. The first three lines correspond to the name of the scheme (in bold), the purpose of each module, and the variables (in italics) used in this module. CCN = cloud condensation nuclei; IFN = ice freezing nuclei.

modeling is part of the ECMWF Integrated Forecasting System (IFS), and 6-hr analyses of aerosol mass mixing ratio are available. The mass mixing ratio of three bins of sea salt aerosols and dust, and one bin of sulfate, hydrophilic, and hydrophobic black carbon and organic matter are predicted (Morcrette et al., 2009). When the aerosol scheme is not activated, the aerosol population of the LIMA microphysics scheme is directly initialized from the MACC analysis. A single bin is considered in MACC for sulfate, hydrophobic organic matter, hydrophobic black carbon, hydrophilic organic matter, and hydrophilic black carbon. Thus, the mass mixing ratio is converted to number concentration to be used in LIMA. Sulfate, hydrophilic black carbon and organic matter, and hydrophobic black carbon and organic matter are transferred into the interstitial CCN, coated CCN, and IFN variables, respectively. For sea salt and dust aerosols, three bins are available in MACC analysis. The three bins of sea salt aerosols are summed, converted to number concentration and transferred into the LIMA interstitial CCN variable associated with sea salt chemical and mean-dimensional properties. The same procedure is used for dust aerosols to be transferred into the LIMA interstitial CCN variable associated with the chemical and mean-dimensional properties of dust.

If the aerosol-microphysics coupling is activated for aerosols of natural origin, the aerosol initialization must be adapted (Figure 3). In this study, sulfate, hydrophilic organic matter and black carbon, and hydrophobic organic matter and black carbon are not handled by the aerosol scheme. Therefore, they are initialized as described previously; that is, their number concentration in LIMA is directly computed from their mass mixing ratio in MACC analysis. Concerning dust particles, the mean radius of the three bins in MACC and of the three modes in ORILAM match quite well. Then the mass of the three individual bins is transferred directly into the three individual modes and converted in terms of moments. For sea salt aerosols, three bins are available in MACC analysis, while five modes are used in ORILAM. The sea salt aerosols emission function of Ovadnevaite et al. (2014) covers a larger range of sea salt aerosols radii than the MACC analysis. The smaller sea salt aerosols mode in ORILAM is supposed to be nonefficient for CCN activation, and this range of size is not present in the MACC analysis: this mode is not initialized from the MACC analysis. The remaining four larger modes in ORILAM are fed by the three bins of MACC. A given fraction of each bin mass is used to calculate the 0th moment (total aerosol number of the lognormal distribution) of each ORILAM mode. The interstitial CCN and IFN variables associated with sea salt and dust aerosols in LIMA are then initialized through ORILAM as described in section 3.3.

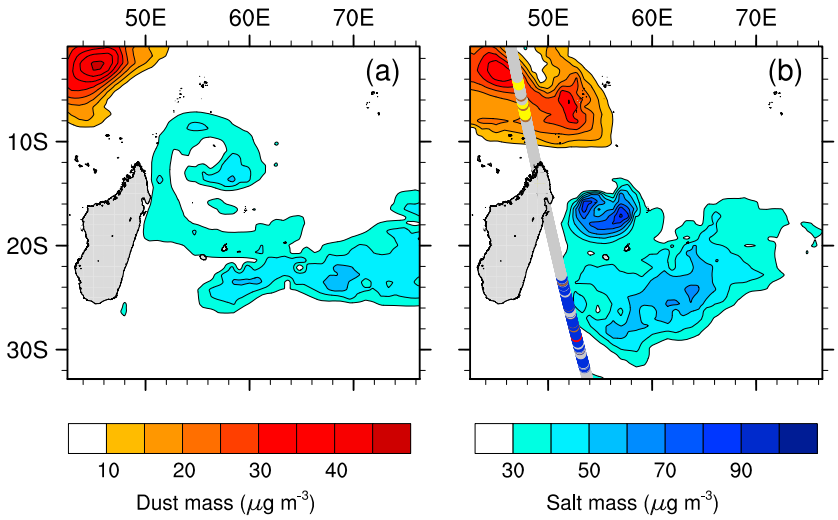

Figure 3. Dust (orange to red colors) and sea salt (blue colors) aerosol mass concentration ($\mu g/m^3$) at 1,400 m altitude on (a) 1 January 2013 at 00 UTC and (b) 2 January 2013 at 12 UTC, from the MACC analysis. In (b) the track of the CALIPSO satellite is overlaid and indicates the aerosol classification (yellow for dust aerosols, blue for sea salt, red for polluted continental aerosols, brown for polluted dust, and black for smoke) retrieved from the CALIOP vertical feature mask algorithm at 1,400 m altitude. The gray color corresponds to areas without measurements due to cloud cover. MACC = Monitoring Atmospheric Composition and Climate project analysis; CALIPSO = Cloud-Aerosol Lidar and Infrared Pathfinder Satellite Observation; CALIOP = Cloud-Aerosol Lidar with Orthogonal Polarization.

4. Numerical Setup

The model was set up with double two-way nested domains having horizontal grid spacings of 8 (D1) and 2 (D2) km with grid sizes of 450 × 450 and 400 × 584 points, respectively (Figure 1a). In the vertical, 70 levels were used, with highest resolution near the surface.

The simulations started on 1 January 2013 at 00 UTC and ended on 3 January 2013 at 03 UTC. The 6-hr ECMWF operational analyses were used to initialize Meso-NH and to provide the lateral boundary inflow conditions. A first segment of the simulation with the larger domain D1 was run for 24 hr. After this time, the higher resolution domain D2 was introduced, encompassing the tropical cyclone inner core and rainbands for the next 27 hr. In the inner domain, deep convection is explicitly resolved, whereas it is parameterized in the outer domain (Bechtold et al., 2001). A shallow convection parameterization (Bechtold et al., 2001) was used in both the inner and outer domains. In the two domains, the turbulence parameterization was based on a 1.5-order closure (Cuxart et al., 2000) with purely vertical turbulent flux computations using the mixing length of Bougeault and Lacarrère (1989). The radiative scheme was the one used at ECMWF (Gregory et al., 2000) including the Rapid Radiative Transfer Model (RRTM) parameterization (Mlawer et al., 1997).

The two-moment microphysics scheme was used and was coupled with the aerosol scheme for sea salt and dust aerosols as described in section 3. ORILAM was used as a one-moment mode (fixed radius and standard deviation). Aerosols were initialized by the 6-hr MACC analysis from ECMWF which also monitored the lateral boundary conditions of the aerosol fields. In this study, the Meso-NH atmospheric model was not coupled to a wave model. Thus, the significant height of the wave that is part of the sea salt aerosols emission function was extracted from the 6-hr ECMWF analysis and interpolated at each time step.

The surface-atmosphere interactions were driven by the surface modeling platform SurFex (Masson et al., 2013). The iterative method of Fairall et al. (1996), revised by Lebeaupin et al. (2006), was used to parameterize the sea fluxes.

In order to highlight the importance of aerosol-microphysics coupling in tropical cyclone modeling, two additional simulations were performed as a complement to the reference simulation (hereafter referred to as 2MA). First, the one-moment microphysics scheme ICE3 (Pinty & Jabouille, 1998) was used (hereafter referred to as 1M). This scheme, derived from Lin et al. (1983), predicts the mixing ratio of five hydrometeor species:

cloud droplets, rain, cloud ice, snow, and graupel. Then, the LIMA microphysics scheme was used without ORILAM (hereafter referred to as 2M). In the latter simulation, the interstitial CCN/IFN in LIMA were initialized and refreshed at the lateral boundaries with the MACC analysis as described in Vié and Pinty (2014), but no aerosol replenishment from the surface was considered in the domain during the simulation. An additional simulation has been performed with the two-moment microphysics scheme with a fixed CCN source. A sea salt aerosol source was homogeneous over the whole domain. The concentration was 100 cm^{-3} between the surface and 1,000 m altitude, then decreased with height, to mimic a clean maritime environment. The track, intensity, and structure of the simulated tropical cyclone were very similar to the ones simulated with the one-moment microphysics scheme. Indeed, LIMA was built upon ICE3; thus, the two schemes share the same parameterizations of the microphysical processes. Then using LIMA with a constant and homogeneous CCN source (therefore with no limitation of the CCN number) roughly comes back to using the ICE3 scheme. Consequently, the results of this simulation are not shown here.

5. Results From the Reference Simulation

The model performance in the configuration "aerosol-microphysics coupled system" (2MA) is analyzed in this section. The aerosol distribution of the environment is first examined. Then, the ability of the model to simulate the tropical cyclone evolution and structure is analyzed.

5.1. Aerosol Distribution

Figure 3 shows the sea salt and dust aerosol mass concentrations at 1,400 m altitude from MACC analysis on 1 January 2013 at 00 UTC, that is, at the beginning of the simulation, and on 2 January 2013 at 12 UTC during a CALIPSO (Cloud-Aerosol Lidar and Infrared Pathfinder Satellite Observations; Winker et al., 2003) satellite overpass. The altitude of 1,400 m was chosen because it corresponds to the core of a dusty air mass that is visible in both MACC analysis and CALIPSO data.

The signature of the high surface winds in the eyewall of Dumile is visible northeast of Madagascar in Figure 3a. At the beginning of the simulation, the highest mass concentration of sea salt aerosols (~50 $\mu g/m^3$) is found in a band centered around 22°S, southeast of the Mascareignes archipelago. This is due to a rough sea driven by strong trade winds from 27 to 31 December, as suggested by the ECMWF wave model analysis (not shown). Thirty-six hours later (Figure 3b), the mass concentration of the sea salt aerosols, emission of which is associated with the strong winds of tropical cyclone Dumile, has significantly increased due to the intensification of the system. The sea salt aerosol mass concentration is more than twice as high as on 1 January at 00 UTC and exceeds 100 $\mu g/m^3$ in some parts of the eyewall. The mass of sea salt aerosols generated by the swell south of the domain has moved westward. It is located south of Dumile but now the mass concentration of sea salt aerosols generated by the storm is higher. The CALIOP (Cloud-Aerosol Lidar with Orthogonal Polarization) vertical feature mask product confirms that sea salt aerosols are the main type of aerosols at 1,400 m altitude in the south of the domain, in agreement with the sea salt aerosols generated by the high trade winds in IFS. Due to the presence of clouds, no data was available between 10°S and 23°S (gray color along the satellite track). Consequently, the sea salt aerosols emitted by the strong cyclonic winds were probably not sampled because of the cirrus cloud coverage.

On 1 January at 00 UTC, a dust plume was located 1,000 km northeast of Madagascar (Figure 3a). Thirty-six hours later, the outflow of dust was transported southward by the monsoon flow and reached the northern part of Madagascar (Figure 3b). The MACC data at larger scale indicated that the sources of this dusty air mass were mainly located in East Africa with a secondary contribution from the Middle East (not shown). The presence of dust aerosol in the environment of Dumile was confirmed by the CALIOP vertical feature mask product, showing that this type of aerosol prevailed in the northwestern part of the domain, between the equator and 10°S, north of Dumile.

On 2 January 2013 at 12 UTC, polluted continental aerosols were observed along the CALIPSO track (Figure 3b) and were probably emitted in Madagascar. However, because of the large predominance of natural aerosols (sea salts and dust), it was assumed that Dumile evolved in a clean maritime environment. This is supported by the conclusions of Duflot et al. (2011), who found a clean maritime environment in this region out of the biomass burning season (July–October).

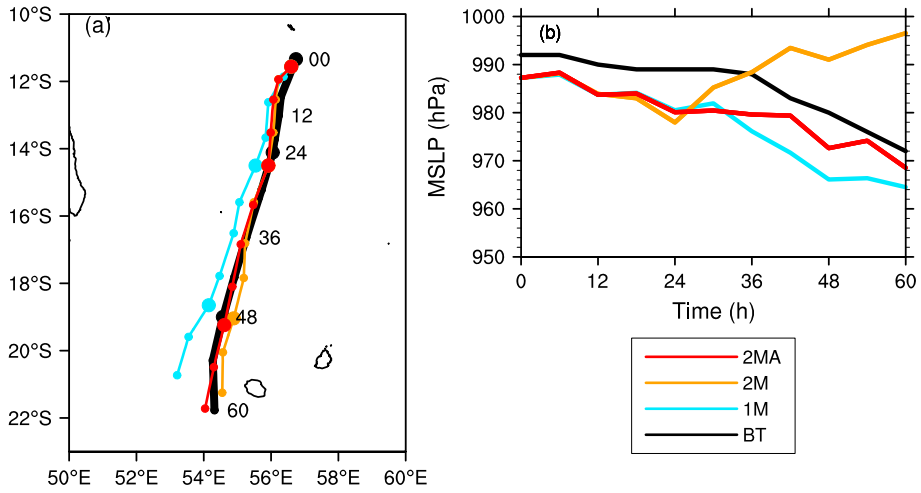

Figure 4. (a) Trajectory and (b) evolution of the minimum sea level pressure (MSLP, hPa) of tropical cyclone Dumile from the best-track (BT) and simulated with Meso-NH.

5.2. Storm Track and Intensity

Figure 4a shows the trajectory of Dumile from the reference simulation (red line) and the best track from RSMC La Réunion (black line). Meso-NH with the ORILAM-LIMA coupling reproduces the trajectory of Dumile well. During the first 24 hr, the simulated track is 30 km to the west of the best track. After this 24-hr spin-up period, the across-track error becomes very low. The simulation is 1 to 2 hr in advance compared to the best track, but this lag was already present at the beginning of the simulation.

Meso-NH tended to overestimate the intensity of Dumile throughout the studied period (Figure 4b). The MSLP was 2 to 10 hPa lower in the 2 MA simulation than in the best track. However, a 4.5-hPa bias in the intensity was already present at the initial state. The rate of intensification was well reproduced by the model (20 hPa in 60 hr for the best track versus 19 hPa in 60 hr in 2MA).

5.3. Storm Structure

The evolution of the storm structure was analyzed through the surface horizontal wind and graupel mixing ratio (Figure 5) at 3 times that were representative of the different stages of the system. On 2 January at 06 UTC (Figure 5a), the surface winds of the tropical storm showed strong asymmetry. Surface winds approached 28 m/s in some eastern parts of the system, but stayed lower than 19 m/s in its western part. The deep convection, represented by the presence of graupel at 6-km altitude, was 150 km from the center and was mainly seen to the north of the system (Figure 5d). A precipitating band was already reaching La Réunion on 1 January as confirmed by satellite images and meteorological stations (Caroff et al., 2014).

Fifteen hours later, horizontal surface winds faster than 22 m/s encircled the eye of the system, with values exceeding 28 m/s in the western and southern parts of the inner core (Figure 5b). Figure 5e clearly shows that deep convection moved closer to the storm center and was mainly found in the southern and southwestern parts of the system. Graupel mixing ratios of up to 4 g/kg were found locally to the south of the system center. Meso-NH was able to capture the observed transition from a monsoon depression to a more typical tropical storm structure.

On 3 January at 09 UTC, Dumile was grazing La Réunion. Deep convection was mainly active in the front and left quadrants of the system (Figure 5f). The strongest winds, exceeding 31 m/s were located in the eastern part of the cyclone (Figure 5c). This is in agreement with the wind gusts of over 100 km/hr recorded on the western and northern coastal regions of La Réunion (137 km/hr in Le Port and 108 km/hr in Saint Gilles).

5.4. Ice Water Content

The ice distribution inside the storm was investigated using the DARDAR product (Delanoë & Hogan, 2010). This product takes advantage of the combination of radar and lidar signals, that is, the high sensitivity to low

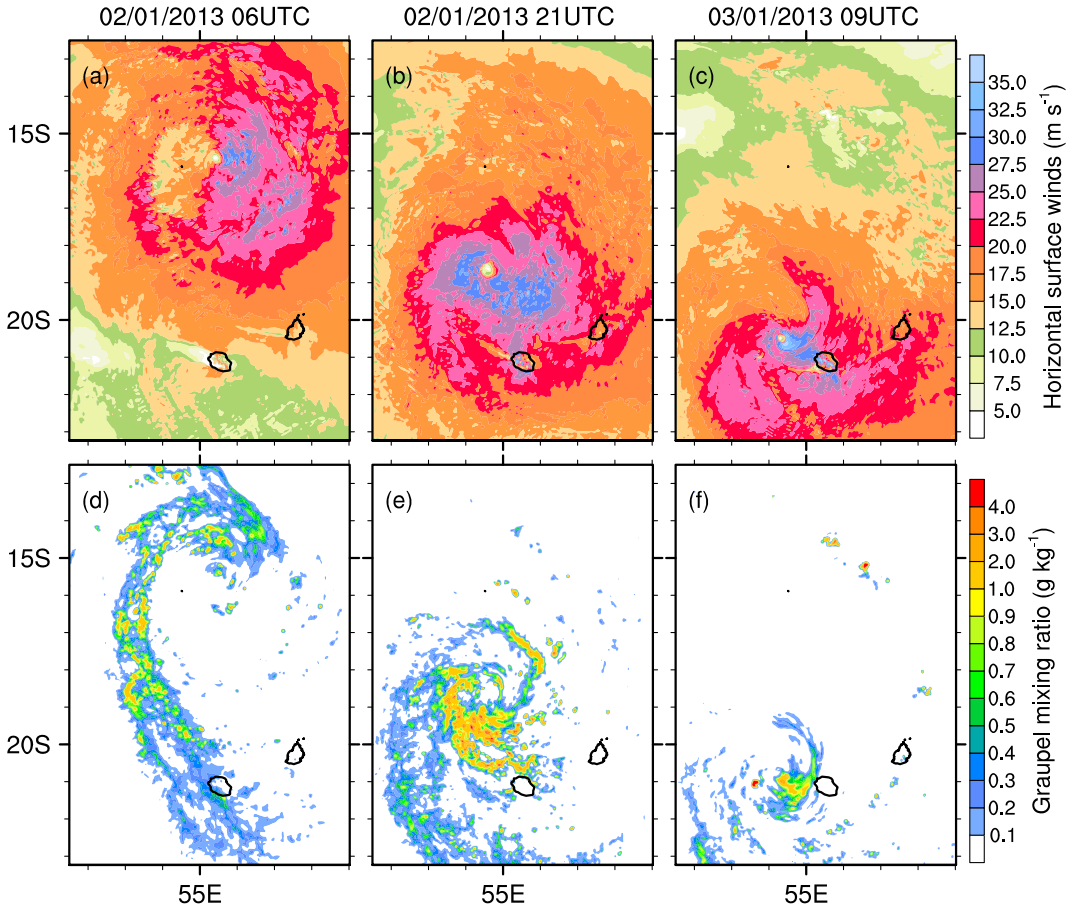

Figure 5. Horizontal surface wind (m/s; a–c), and graupel mixing ratio at 6,000-m altitude (g/kg; d–f) on 2 January at 06 UTC (left), 2 January at 21 UTC (middle), and 3 January at 09 UTC (right).

ice water content of the lidar and the fairly weak attenuation of the radar in ice clouds (even for optical depths larger than 3). The Varcloud algorithm (Delanoë & Hogan, 2008) uses a variational approach combining CALIOP/CALIPSO (Winker et al., 2010) lidar, CloudSat Cloud Profiling Radar (Stephens et al., 2002), and the radiometer data on board MODIS. This product allows ice cloud properties to be retrieved in the whole tropospheric column.

On 1 January at 09 UTC, the A-Train satellites passed over the cirrus clouds east of the inner core of Dumile and a primary outer rainband south of the system (Figure 6d). The ice water content (IWC) was retrieved from the DARDAR-CLOUD product (Figure 6c) and was extracted from Meso-NH (Figure 6a) along the same section (Figure 6b). Two distinct structures can be distinguished in the IWC profiles of DARDAR and Meso-NH. Between 23°S and 14°S, in the outer rainband, high IWC values are found both in the model and in the observations. DARDAR IWC exceeds 0.1 g/m^3 between 4.5- and 11-km altitude, in the convective cores. Note that convective cores are strongly affected by multiple scattering and the radar measurements must be used cautiously. Multiple scattering could artificially enhance the reflectivity, leading to an overestimation of the IWC. Meso-NH simulates similar values but between 4.5- and 9-km altitude. Values up to 5×10^{-2} g/m^3 are found between 9 and 12 km both in the DARDAR retrieval and in the Meso-NH simulation. The cirrus clouds between 15°S and 3°S are 2–4 km thick according to IWC values retrieved with DARDAR between 1×10^{-2} and 5×10^{-2} g/m^3 (Figure 6c). In comparison with DARDAR, Meso-NH generally tends to underestimate the extension of high IWC values in the cirrus clouds. IWC values in Meso-NH are spread over a larger range of values (1×10^{-4} to 5×10^{-2} g/m^3).

The version 2.1 of DARDAR-CLOUD was used in this study. It has been found that the extinction-to-backscatter a priori information was incorrect for very cold temperatures. This a-priori issue leads to an

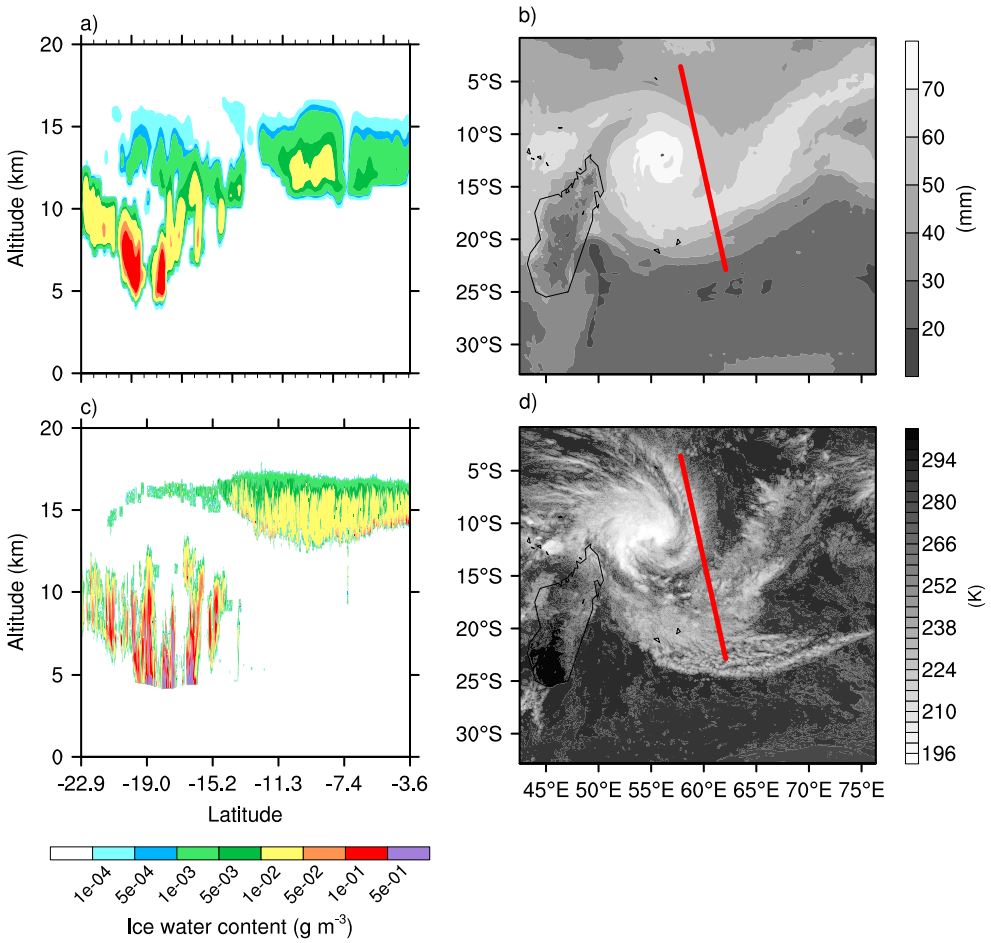

Figure 6. Vertical profiles of the ice water content (g/m^3; a) simulated by Meso-NH with the 2 MA configuration and (c) retrieved from DARDAR on 1 January 2013 at 09 UTC. (b) Water vapor thickness from Meso-NH (mm) and (d) IR brightness temperature (K) from Meteosat 7. The vertical cross section is taken along the red segment shown in (b) and (d) for Meso-NH and DARDAR, respectively. Meso-NH = non-hydrostatic mesoscale atmospheric model; DARDAR = raDAR/liDAR.

overestimation of the extinction when only lidar is used. This can explain a slight overestimation of IWC for cirrus clouds which was reported by Deng et al. (2013) when comparing DARDAR-CLOUD IWC against in situ data and other retrievals. Note that this overestimation occurs only if there is no molecular signal beyond the cloud and therefore this signal cannot be used as an extra constraint (Delanoë & Hogan, 2010). Combined to uncertainties on the particle size distribution and mass-diameter relationship both in the Meso-NH simulation and in the satellite retrieval could explain the divergences between the IWC from the model and that retrieved from satellite observations. Overall, Meso-NH provides good reproduction of the ice water content distribution and amount in the convective core of a rainband and the cirrus clouds next to the inner core of Dumile.

6. Sensitivity to Aerosol-Microphysics Coupling

In order to highlight the importance of aerosol-microphysics coupling in tropical cyclone modeling, the two additional simulations are compared to the reference simulation in this section. First, the impact of using a coupled aerosol-microphysics scheme instead of a simple one-moment microphysics scheme, as usually implemented in numerical weather prediction models, is investigated through the comparison between 1M and 2MA. Then the impact of using an aerosol scheme along with a two-moment microphysics scheme is analyzed by comparing 2M and 2MA.

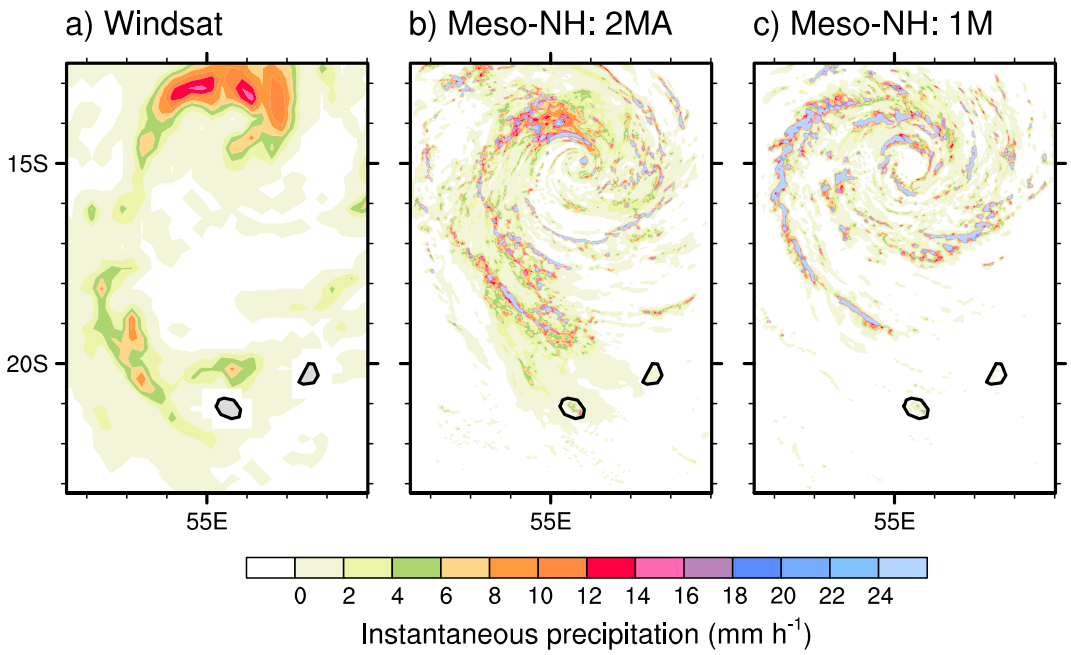

Figure 7. Instantaneous precipitation (mm/hr) on 2 January at 03 UTC, (a) retrieved from Windsat and from Meso-NH in the (b) 2 MA and (c) 1 M configurations. Meso-NH = non-hydrostatic mesoscale atmospheric model.

6.1. One-Versus Two-Moment Microphysical Schemes

Figure 4 shows significant differences in the track and intensity of Dumile in 1M and 2MA. The across-track error in 1M is a few tens of kilometers to the west, while the track of 2MA is very close to the best track (Figure 4a). In terms of intensity, the tropical cyclone intensifies during the 60 hr of both simulations (Figure 4b). However, the two simulations start to diverge after 30 hr: 1M becomes 4–9 hPa more intense than 2MA. Thus, 1M and 2MA differ both in track and intensity. The possible origins of such discrepancies are now analyzed.

Figure 7 represents the instantaneous precipitation rate given by the simulations and estimated from the polarimetric microwave radiometer Windsat on board Coriolis on 2 January at 09 UTC. The retrieval relies on several channels from 10 to 37 GHz (Li et al., 2008). The higher precipitation rates retrieved from Windsat are concentrated in the northern quadrant of the eyewall (8–16 mm/hr) and in a rainband located northeast of La Réunion (4–8 mm/hr; Figure 7a). The 2MA simulation (Figure 7b) reproduces the strong precipitation pattern north of the eyewall, with maximum rates around 20 mm/hr. The southwestern rainband is simulated by 2MA but is located northeast of its observed position. The 2MA generates a narrow rainband at 17°S that was not observed, but the observed low precipitation rates ($<$4 mm/hr) are well simulated. The precipitation rates generated by 1M (Figure 7c) diverge more noticeably from the observations. Even though the higher precipitation rates in the eyewall are found in the northern quadrant as observed, precipitation is produced all around the eye. The 1M generates almost exclusively high rain rates ($>$20 mm/hr) concentrated over narrow regions and underestimates the low precipitation rates ($<$4 mm/hr). So, compared to 1M, the 2MA precipitation field exhibits a more asymmetric pattern and manages to produce realistic rainbands and low rain rates, as observed.

This difference in the tropical cyclone symmetry between 2MA and 1M is also evident in the horizontal wind structure. Figure 8a shows the evolution of the 47-kt wind speed extent in each quadrant of the system. In 1M, up to 30 hr, the 47-knot wind speed extent varies between 0 and 200 km depending on the quadrant. After 30 hr, the four curves converge and the 47-kt wind speed extent per quadrant lies between 130 and 190 km. The tropical cyclone in 1M develops a more symmetric structure after 36 hr. In 2MA, the strong asymmetry in the 47-kt wind speed structure remains until the end of the simulation. The mean 47-kt wind speed extent increases throughout the simulation, and is 20 to 90 km higher in 1M (blue dots) than in 2MA. Concerning the evolution of the 33-kt wind speed extent (Figure 8b), the mean radius is larger in 1M than

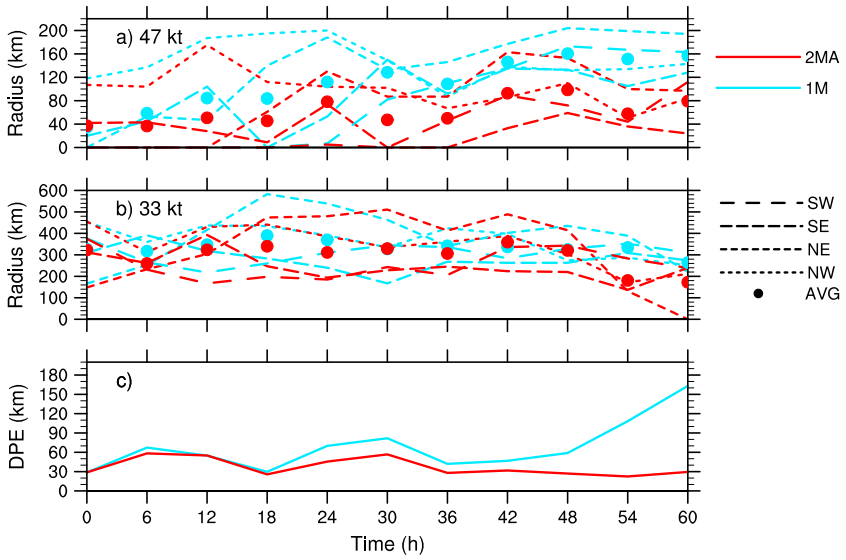

Figure 8. Evolution of (a) the 47-knot (1 knot = 1.85 km/hr) wind speed extent (km), (b) the 33-knot wind speed extent (km), and (c) the direct positional error (DPE, in kilometer) for 1 M (blue) and 2 MA (red). In (a) and (b), the lines represent the evolution of the 47-knot radius and of the 33-knot radius in the four quadrants, while the dots show the average values.

in 2MA (except at 42 hr) but the gap is not as large as for the 47-kt wind speed radius. Between 42 and 60 hr, the mean 33-kt wind speed extent in 2MA decreases from 350 to 170 km. This decrease is lower in 1M (from 340 to 270 km). In 2MA, there is a significant difference in the 33-kt wind speed extents among the four quadrants throughout the simulation, while these curves converge after 36 hr of simulations in 1M. Therefore, the 33-kt wind speed structure of the tropical cyclone in 1M tends to become more symmetric and larger than in 2MA after 36–42 hr. This difference in the 1M and 2MA wind structure occurs at the same time as an increase in the direct position error (DPE) in 1M (Figure 8c). While the DPE stays below 80 km between 0 and 36 hr of simulation, it starts to increase after 42 hr and reaches 160 km at 60 hr. In contrast to 1M, the DPE in 2MA remains smaller than 60 km throughout the simulation and decreases to 30 km at the end of the simulation.

Using a one-moment microphysics scheme for the simulation of tropical cyclone Dumile leads to a larger and more symmetric system than using a two-moment microphysics scheme coupled with an aerosol scheme. Tropical storms with more intense winds over a large radial distance tend to have a larger inertial stability and to be more resilient with respect to environmental influences. Thus, the motion of these systems would be more sensitive to the beta drift (Fovell et al., 2016; Fovell & Su, 2007), which could partly explain the westward motion of the storm in 1M. The main difference between 1M and 2MA comes from the way cloud droplets and ice crystals are formed. In the one-moment microphysics scheme used in 1M, the formation of cloud droplets is not limited by CCN availability but by thermodynamical conditions (water vapor saturation). However, the main source of CCN for the tropical cyclone in a clean maritime environment comes from sea salt emission by strong cyclonic winds. Therefore, the CCN availability is determined by the location and strength of the horizontal surface winds. This effect can enhance convective asymmetries in the inner core of the system, which could also impact the tropical cyclone motion (Fovell et al., 2016). Several studies have shown that using different microphysics schemes could impact the simulated tropical cyclone intensity through latent heat release associated with microphysical conversions (Khain et al., 2016; Li et al., 2013a; Wang, 2002; Zhu & Zhang, 2006). It is likely that the CCN availability in the LIMA microphysics scheme is also a key point for the horizontal distribution of latent heating profiles.

6.2. Impact of Aerosol-Microphysics Coupling

The importance of careful aerosol processing is illustrated through the comparison between 2MA and 2M. Figure 4a shows that the track of Dumile is very similar in both simulations and reproduces the analyzed track well. However, there are large differences in the evolution of the intensity (Figure 4b). The MSLP evolves in

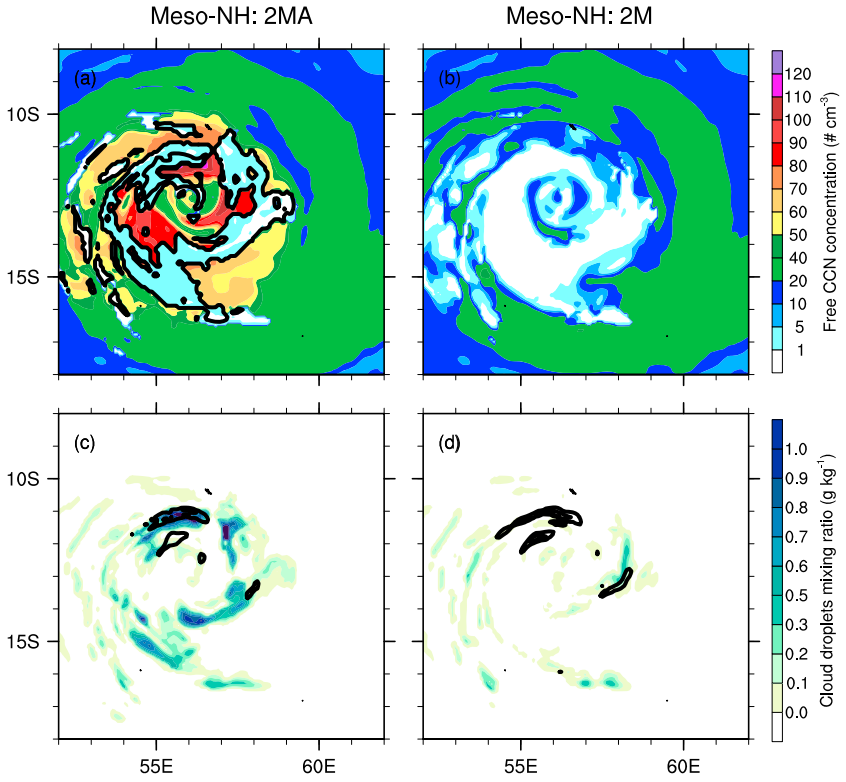

Figure 9. (a, b) Number concentration (cm^{-3}) of interstitial (colors) and activated (black isolines at 50 cm^{-3}) CCN associated with sea salt particles. (c, d) Cloud droplets (colors) and rain (black isolines at 0.5 and 1 g/kg) mixing ratio (g/kg). The horizontal cross sections are taken at 2,000-m altitude on 1 January at 12 UTC for the 2 MA (right) and the 2 M (left) simulations. Meso-NH = non-hydrostatic mesoscale atmospheric model; CCN = cloud condensation nuclei.

the same way in 2M and 2MA during the first 24 hr. Then, the two curves diverge. Throughout the simulation, 2MA continues to intensify at a rate similar to the analyzed one. However, 2M starts to weaken dramatically after 24 hr due to the lack of sea salt aerosol emission to feed the microphysics scheme.

Figure 9 shows the number concentration of sea salt aerosols acting as CCN and the cloud droplets and rain mixing ratio at 2,000-m altitude on 1 January at 12 UTC. In 2MA, the number concentration of interstitial CCN associated with sea salt aerosols peaks in the inner core of the system, with values exceeding 100 cm^{-3} in some regions (Figure 9a). These sea salt aerosols are generated by the strong horizontal winds of the tropical cyclone primary circulation. CCN activation is very efficient in the eyewall and the inner rainband, where the number concentration of the interstitial CCN falls to less than 10 cm^{-3}, while the number concentration of activated CCN exceeds 50 cm^{-3}. In the region with active nucleation, the cloud droplet mixing ratio is between 0.5 and 1 g/kg (Figure 9c). Aerosols are also efficiently removed by wet deposition in this region where raindrops are abundant (not shown). Since the scavenging is less efficient for aerosol particles with diameter between 0.2 and 2 μm (Slinn, 1983), interstitial aerosol particles in this range of values are still available for activation into cloud droplets.

After only 12 hr of simulation, the number concentration of interstitial CCN in 2M is almost zero in the inner core of the system (Figure 9b); all interstitial CCN initially present in the domain being activated or scavenged. In the absence of sea salt emission in 2M, there is no longer a CCN source for cloud droplets to form in the inner core except those transported from the cyclone environment. Relatively low cloud droplet mixing ratios ($<$0.5 g/kg) are found in 2M (Figure 9d). Since there are no longer any interstitial CCN in the inner core region, the cloud droplet concentration is low, which is conducive to particles with larger diameters and thus more prone to coalescence and conversion to raindrops (e.g., Albrecht, 1989; Rosenfeld et al., 2012; Twomey, 1977). In 2M, the raindrop mixing ratio exceeds 1 g/kg at 2,000-m altitude in the northern part of the eyewall, while it is around 0.5 g/kg in 2MA. Even if there are no more CCN to be activated into cloud droplets, the mass of cloud droplets can also be produced

through ice melting and raindrop evaporation. Out of the inner core, the number concentration of interstitial CCN at 2,000-m altitude is between 10 and 30 cm^{-3} in both simulations.

Up to now, kilometer-scale numerical studies dealing with the impact of aerosols on tropical cyclones (Hazra et al., 2013; Herbener et al., 2014; Khain et al., 2008, 2010, 2016; Lynn et al., 2016; Rosenfeld et al., 2012; Wang et al., 2014) have used more or less homogeneous aerosol fields with concentrations that decrease with height in the domain and at the initial state. Most of the time, arbitrarily fixed aerosol concentrations representative of clean maritime, clean continental, or polluted continental values are supplied at the lateral boundaries and advected under favorable wind conditions. However, the local production of sea salt aerosols, which are considered as the most efficient CCN (e.g., Andreae & Rosenfeld, 2008; O'Dowd et al., 1999) is not considered in these studies, except in Wang et al. (2014). Sea salt aerosols are produced at the sea surface by bubble bursting during wave breaking (Blanchard, 1963) and by the tearing of wave crests at high wind speeds (Monahan et al., 1986). Thus, they should be preferentially produced in the inner core of the cyclone where the strongest surface winds and waves are encountered. Therefore, even if aerosols are transported toward the storm by the flow, they can be activated into cloud droplets in the outer and inner rainbands before reaching the eyewall (Khain et al., 2016; Lynn et al., 2016; Rosenfeld et al., 2012). Under clean maritime conditions, this hypothesis of a continuous aerosol source supplied by advection from the lateral boundaries cannot be sustained. Moreover, most of the previous studies did not consider aerosol scavenging while it could prevent aerosol particles from the environment to be ingested in the inner core. This result shows that it is important to explicitly take account of the local production of sea salt aerosols associated with the high winds and waves in tropical cyclones to reproduce the aerosol-microphysics-dynamics interactions. It is important especially when performing simulations of long-lasting systems that need to generate their own condensation nuclei in clean atmosphere conditions.

7. Conclusions

In this paper, the coupling between the lognormal aerosol scheme ORILAM (Tulet et al., 2005) and the two-moment microphysics scheme LIMA (Vié et al., 2016) implemented in the Meso-NH model is presented. A realistic aerosol field is initialized with the MACC analysis, which is also used for the lateral boundary conditions. A parameterization of the sea salt aerosol emission by high winds and waves (Ovadnevaite et al., 2014) is also considered. These new features are illustrated through the simulation of the tropical cyclone Dumile that evolved in the South-West Indian Ocean in 2013. The reference simulation using the aerosol-microphysics coupled system (2MA) represents the analyzed track and intensity well. The simulated structure of Dumile (rainband position, ice water content in convective and cirrus clouds, convection, and wind asymmetries) also shows fairly good agreement with satellite observations (Meteosat, Windsat, CALIPSO and Cloudsat).

Several simulations were performed to analyze the advantages of such a coupled scheme. Using a one-moment microphysics scheme tends to produce a more intense and more symmetrical tropical cyclone. It also displays higher winds over a large radial distance, which make it more resilient with respect to external forcing. It is assumed that, because of the beta drift, its track deviates to the west of the analyzed trajectory. Moreover, the production of sea salt aerosols (acting as the main source of CCN here) in regions with high winds and waves may induce or amplify convective asymmetries, which could also impact the storm track. On the contrary, in the one-moment scheme, aerosols are supposed to be inexhaustible and available homogeneously over the domain.

In contrast, using a two-moment microphysics scheme alone without sea salt aerosol regeneration at each time step leads to a dramatic weakening of the tropical storm after 24 hr of simulation. This is due to the rapid consumption of almost all interstitial CCN in the inner core of the system. Cloud droplet production drops off in the inner core. The production of cloud droplets in the outer rainbands and the supply of interstitial CCN through the lateral boundaries are not sufficient to maintain the cyclone structure and the intensity thus collapses rapidly. A two-moment microphysics scheme where interstitial CCN are supplied by an aerosol scheme represents the interaction between the tropical cyclone and its source of cloud particles better in terms of numbers and location. Hence, it is necessary to take the aerosol-microphysics interactions into account to improve the tropical cyclone track, intensity, and structure in numerical simulations at kilometer-scale resolution.

However, several limitations of this study must be pointed out and should be solved in future studies. First, a bulk scheme was used in this study. As reviewed by Khain et al. (2015) and Fan et al. (2016), bulk schemes are less adapted than bin schemes for aerosol-cloud interactions study. The main criticisms about bulk schemes are that most of them do not include a CCN budget, assume the saturation adjustment and use average fall velocities. Bin schemes allow to describe the microphysical processes with more accuracy, and no a priori information about the particle size distribution is needed. However, their extremely high computational cost prevents them from being used over large domains during long periods of time and in operational models. Despite their accuracy, these schemes are limited by the lack of theoretical understanding of cloud microphysics (Fan et al., 2016). In this context, it was decided to use a new two-moment bulk scheme coupled with an aerosol budget. Second, as stated by Vié and Pinty (2014), some uncertainties lie in the conversion between the aerosol mass from MACC and the number concentration in ORILAM or LIMA. This step should be better evaluated and calibrated. Nevertheless, despite some uncertainties in the aerosol number concentration, the 3-D MACC analysis provides realistic aerosol distributions to serve as initial state and boundary conditions over this basin. Third, the coupling between the atmospheric model Meso-NH, an oceanic model and a wave model is not considered. The coupling with an oceanic model is important since the ocean–atmosphere heat and humidity fluxes are considered as the fuel of the tropical cyclone and, in turn, the tropical cyclone modifies the ocean temperature and currents (Black et al., 2007; D'Asaro et al., 2014, and references therein). In addition, the sea salt emission parameterizations depend not only on the wind speed but also on the sea surface temperature and the significant wave height (e.g., Grythe et al., 2014). In the case of Dumile, the ECMWF analysis was in a very good agreement with the best track data. Consequently, the wave field extracted from ECMWF analysis was in rather good agreement with the Meso-NH surface wind field (not shown), despite a probable underestimation due to the lower resolution of IFS. Moreover, Dumile moved rather fast (at ~20–25 km/hr), which limited the negative feedback of the ocean surface cooling (Mei et al., 2012).

In this study, the effect of sea spray on the momentum, heat, and moisture flux was not considered. However, Andreas (2004) showed that sea spray reduce the air-sea momentum flux at high winds. Through the latent heat absorption and water vapor release during evaporation, sea sprays also modify the enthalpy flux (Wang et al., 2001). In a series of papers, Shpund et al. (2011, 2012, 2014) performed large eddy simulations (LES) of the marine boundary layer under strong wind, using a spectral bin microphysics including the effects of sea spray. They highlighted the role of large eddies of the hurricane mixed layer in transporting part of the large sea spray aerosols upward, toward the cloud base, which could influence the microphysical structure of the cloud.

An ocean-waves-atmosphere coupled system (Pianezze et al., 2018; Voldoire et al., 2017) will be deployed in future studies of tropical cyclones in addition to the aerosol-microphysics coupling presented in this paper. The structure and variation of intensity of some intense tropical cyclones that have propagated in the South-West Indian Ocean recently (e.g., Fantala in April 2016 or Enawo in March 2017) will be examined next, using a fully coupled system.

Acknowledgments
This work was partly funded by the French national program LEFE/INSU and by the French CNES/TOSCA project SOLID. Computer resources were allocated by GENCI (project 6660). This work was done during the PhD of T. Hoarau who was financially supported by the Réunion Region and the European Union Council. The Meso-NH code is publicly available at http://www.mesonh.aero.obs-mip.fr/. The model development and the simulations were made with version 5-1-4; the modifications brought to the ORILAM and LIMA schemes are available upon request from C. Barthe and next in a future version of Meso-NH. The MACC analysis can be obtained from http://www.gmes-atmosphere.eu/. Data concerning tropical cyclone Dumile are available on the Web site of RSMC La Réunion (http://www.meteo.fr/temps/domtom/La_Reunion/webcmrs9.0/#). We also acknowledge ICARE Data and Services Center (http://www.icare.univ-lille1.fr) for providing CALIPSO and DARDAR-CLOUD data.

References

Albrecht, B. A. (1989). Aerosols, cloud microphysics, and fractional cloudiness. *Science*, *245*(4923), 1227–1230. https://doi.org/10.1126/science.245.4923.1227

Andreae, M. O., & Rosenfeld, D. (2008). Aerosol-cloud-precipitation interactions. Part 1. The nature and sources of cloud-active aerosols. *Earth-Science Reviews*, *89*(1-2), 13–41. https://doi.org/10.1016/j.earscirev.2008.03.001

Andreas, E. L. (2004). Spray stress revisited. *Journal of Physical Oceanography*, *34*, 1429–1440. https://doi.org/10.1175/1520-0485(2004)034<1429:SSR>2.0.C0;2

Aouizerats, B., Thouron, O., Tulet, P., Mallet, M., Gomes, L., & Henzing, J. S. (2010). Development of an online radiative module for the computation of aerosol optical properties in 3-D atmospheric models: Validation during the EUCAARI campaign. *Geoscientific Model Development*, *3*(2), 553–564. https://doi.org/10.5194/gmd-3-553-2010

Baray, J.-L., Clain, G., Plu, M., Feld, E., & Caroff, P. (2010). Occurrence of monsoon depressions in the Southwest Indian Ocean: Synoptic descriptions and stratosphere to troposphere exchange investigations. *Journal of Geophysical Research*, *115*, D17108. https://doi.org/10.1029/2009JD013390

Barthe, C., Hoarau, T., & Bovalo, C. (2016). Cloud electrification and lightning activity in a tropical cyclone-like vortex. *Atmospheric Research*, *180*, 297–309. https://doi.org/10.1016/j.atmosres.2016.05.023

Bechtold, P., Bazile, E., Guichard, F., Mascart, P., & Richard, E. (2001). A mass-flux convection scheme for regional and global models. *Quarterly Journal of the Royal Meteorological Society*, *127*(573), 869–886. https://doi.org/10.1002/qj.49712757309

Berthet, S., Leriche, M., Pinty, J.-P., Cuesta, J., & Pigeon, G. (2010). Scavenging of aerosol particles by rain in a cloud resolving model. *Atmospheric Research*, *96*(2–3), 325–336. https://doi.org/10.1016/j.atmosres.2009.09.015

Black, P. G., D'Asaro, E. A., Sanford, T. B., Drennan, W. M., Zhang, J. A., French, J. R., et al. (2007). Air–sea exchange in hurricanes: Synthesis of observations from the coupled boundary layer air–sea transfer experiment. *Bulletin of the American Meteorological Society*, *88*(3), 357–374. https://doi.org/10.1175/BAMS-88-3-357

Blanchard, D. C. (1963). The electrification of the atmosphere by particles from bubbles in the sea. *Progress in Oceanography*, *1*, 73–202. https://doi.org/10.1016/0079-6611(63)90004-1

Bougeault, P., & Lacarrère, P. (1989). Parameterization of orography-induced turbulence in a mesobeta-scale model. *Monthly Weather Review*, *117*(8), 1872–1890. https://doi.org/10.1175/1520-0493(1989)117<1872:POOITI>2.0.CO;2

Caroff, P., Bientz, C., Boudart, G., Dupont, T., Langlade, S., & Quételard, H. (2014). *Cyclone season South-West Indian Ocean 2012–2013* (p. 112). Saint-Denis, La Réunion: Météo-France/Direction Interrégionale de La Réunion.

Carrio, G. G., & Cotton, W. R. (2011). Investigations of aerosol impacts on hurricanes: Virtual seeding flights. *Atmospheric Chemistry and Physics*, *11*(6), 2557–2567. https://doi.org/10.5194/acp-11-2557-2011

Claeys, M. (2016). Modélisation des aérosols marins et de leur impact radiatif direct sur le bassin méditerranéen dans le cadre du projet CHARMEX (PhD thesis, 271 pp.). University of Toulouse.

Cohard, J., Pinty, J.-P., & Bedos, C. (1998). Extending Twomey's analytical estimate of nucleated cloud droplet concentrations from CCN spectra. *Journal of the Atmospheric Sciences*, *55*(22), 3348–3357. https://doi.org/10.1175/1520-0469(1998)055<3348:ETSAEO>2.0.CO;2

Cooper, W. A. (1986). Ice initiation in natural clouds. *Meteorological Monographs*, *21*(43), 29–32. https://doi.org/10.1175/0065-9401-21.43.29

Crumeyrolle, S., Gomes, L., Tulet, P., Matsuki, A., Schwarzenboeck, A., & Crahan, K. (2008). Increase of the aerosol hygroscopicity by aqueous mixing in a mesoscale convective system: A case study from the AMMA campaign. *Atmospheric Chemistry and Physics*, *11*(2), 479–494. https://doi.org/10.5194/acp-11-479-2011

Cuxart, J., Bougeault, P., & Redelsperger, J.-L. (2000). A turbulence scheme allowing for mesoscale and large-eddy simulations. *Quarterly Journal of the Royal Meteorological Society*, *126*(562), 1–30. https://doi.org/10.1002/qj.49712656202

D'Asaro, E., Black, P. G., Centurioni, L. R., Chang, Y., Chen, S. S., Foster, R. C., et al. (2014). Impact of typhoons on the ocean in the Pacific. *Bulletin of the American Meteorological Society*, *95*(9), 1405–1418. https://doi.org/10.1175/BAMS-D-12-00104.1

Delanoë, J., & Hogan, R. J. (2008). A variational scheme for retrieving ice cloud properties from combined radar, lidar, and infrared radiometer. *Journal of Geophysical Research*, *113*, D07204. https://doi.org/10.1029/2007JD009000

Delanoë, J., & Hogan, R. J. (2010). Combined CloudSat-CALIPSO-MODIS retrievals of the properties of ice clouds. *Journal of Geophysical Research*, *115*, D00H29. https://doi.org/10.1029/2009JD012346

Deng, M., Mace, G. G., Wang, Z., & Lawson, R. P. (2013). Evaluation of several A-train ice cloud retrieval products with in situ measurements collected during the SPARTICUS campaign. *Journal of Applied Meteorology and Climatology*, *52*(4), 1014–1030. https://doi.org/10.1175/JAMC-D-12-054.1

Duflot, V., Royer, P., Chazette, P., Baray, J.-L., Courcoux, Y., & Delmas, R. (2011). Marine and biomass burning aerosols in the southern Indian Ocean: Retrieval of aerosol optical properties from shipborne lidar and Sun photometer measurements. *Journal of Geophysical Research*, *116*, D18208. https://doi.org/10.1029/2011JD015839

Fairall, C. W., Bradley, E. F., Rogers, D. P., Edson, J. B., & Young, G. S. (1996). Bulk parameterization of air-sea fluxes for Tropical Ocean-Global Atmosphere Coupled-Ocean Atmosphere Response Experiment. *Journal of Geophysical Research*, *101*(C2), 3747–3764. https://doi.org/10.1029/95JC03205

Fan, J., Wang, Y., Rosenfeld, D., & Liu, X. (2016). Review of aerosol-cloud interactions: Mechanisms, significance, and challenges. *Journal of the Atmospheric Sciences*, *73*(11), 4221–4252. https://doi.org/10.1175/JAS-D-16-0037.1

Fletcher, N. H. (1962). *The physics of rain clouds* (p. 386). New York: Cambridge University Press.

Fovell, R. G., Bu, Y. P., Corbosiero, K. L., Tung, W., Cao, Y., Kuo, H., et al. (2016). Influence of cloud microphysics and radiation on tropical cyclone structure and motion. *Meteorological Monographs*, *56*, 11.1–11.27. https://doi.org/10.1175/AMSMONOGRAPHS-D-15-0006.1

Fovell, R. G., Corbosiero, K. L., & Kuo, H. (2009). Cloud microphysics impact on hurricane track as revealed in idealized experiments. *Journal of the Atmospheric Sciences*, *66*(6), 1764–1778. https://doi.org/10.1175/2008JAS2874.1

Fovell, R. G., Corbosiero, K. L., Seifert, A., & Liou, K.-N. (2010). Impact of cloud-radiative processes on hurricane track. *Geophysical Research Letters*, *37*, L07808. https://doi.org/10.1029/2010GL042691

Fovell, R. G., & Su, H. (2007). Impact of cloud microphysics on hurricane track forecasts. *Geophysical Research Letters*, *34*, L24810. https://doi.org/10.1029/2007GL031723

Franklin, C. N., Holland, G. J., & May, P. T. (2005). Sensitivity of tropical cyclone rainbands to ice-phase microphysics. *Monthly Weather Review*, *133*(8), 2473–2493. https://doi.org/10.1175/MWR2989.1

Gregory, D., Morcrette, J.-J., Jakob, C., Beljaars, A. C. M., & Stockdale, T. (2000). Revision of convection, radiation and cloud schemes in the ECMWF integrated forecasting system. *Quarterly Journal of the Royal Meteorological Society*, *126*(566), 1685–1710. https://doi.org/10.1002/qj.49712656607

Grini, A., Tulet, P., & Gomes, L. (2006). Dusty weather forecasts using the MesoNH mesoscale atmospheric model. *Journal of Geophysical Research*, *111*, D19205. https://doi.org/10.1029/2005JD007007

Grythe, H., Ström, J., Krejci, R., Quinn, P., & Stohl, A. (2014). A review of sea-spray aerosol source functions using a large global set of sea salt aerosol concentration measurements. *Atmospheric Chemistry and Physics*, *14*(3), 1277–1297. https://doi.org/10.5194/acp-14-1277-2014

Hallett, J., & Mossop, S. C. (1974). Production of secondary ice particles during the riming process. *Nature*, *249*(5452), 26–28. https://doi.org/10.1038/249026a0

Hazra, A., Mukhopadhyay, P., Taraphdar, S., Chen, J.-P., & Cotton, W. R. (2013). Impact of aerosols on tropical cyclones: An investigation using convection-permitting model simulation. *Journal Geophysical Research: Atmospheres*, *118*, 7157–7168. https://doi.org/10.1002/jgrd.50546

Herbener, S. R., van den Heever, S. C., Carrió, G. G., Saleeby, S. M., & Cotton, W. R. (2014). Aerosol indirect effects on idealized tropical cyclone dynamics. *Journal of the Atmospheric Sciences*, *71*(6), 2040–2055. https://doi.org/10.1175/JAS-D-13-0202.1

Islam, T., Srivastava, P. K., Rico-Ramirez, M. A., Dai, Q., Gupta, M., & Singh, S. K. (2015). Tracking a tropical cyclone through WRF–ARW simulation and sensitivity of model physics. *Natural Hazards*, *76*(3), 1473–1495. https://doi.org/10.1007/s11069-014-1494-8

Jin, Y., Wang, S., Nachamkin, J., Doyle, J. D., Thompson, G., Grasso, L., et al. (2014). The impact of ice phase cloud parameterizations on tropical cyclone prediction. *Monthly Weather Review*, *142*(2), 606–625. https://doi.org/10.1175/MWR-D-13-00058.1

Kärcher, B., & Lohmann, U. (2002). A parameterization of cirrus cloud formation: Homogeneous freezing including effects of aerosol size. *Journal of Geophysical Research*, *107*(D23), 4698. https://doi.org/10.1029/2001JD001429

Khain, A., Lynn, B., & Dudhia, J. (2010). Aerosol effects on intensity of landfalling hurricanes as seen from simulations with the WRF model with spectral bin microphysics. *Journal of the Atmospheric Sciences*, *67*(2), 365–384. https://doi.org/10.1175/2009JAS3210.1

Khain, A., Lynn, B., & Shpund, J. (2016). High resolution WRF simulations of Hurricane Irene: Sensitivity to aerosols and choice of microphysical schemes. *Atmospheric Research*, *167*, 129–145. https://doi.org/10.1016/j.atmosres.2015.07.014

Khain, A. P., Beheng, K. D., Heymsfield, A., Korolev, A., Krichak, S. O., Levin, Z., et al. (2015). Representation of microphysical processes in cloud-resolving models: Spectral (bin) microphysics versus bulk parameterization. *Reviews of Geophysics*, *53*(2), 247–322. https://doi.org/10.1002/2014RG000468

Khain, A. P., BenMoshe, N., & Pokrovsky, A. (2008). Factors determining the impact of aerosols on surface precipitation from clouds: An attempt at classification. *Journal of the Atmospheric Sciences*, *65*(6), 1721–1748. https://doi.org/10.1175/2007JAS2515.1

Lebeaupin, C., Ducrocq, V., & Giordani, H. (2006). Sensitivity of torrential rain events to the sea surface temperature based on high-resolution numerical forecasts. *Journal of Geophysical Research*, *111*, D12110. https://doi.org/10.1029/2005JD006541

Li, J., Wang, G., Lin, W., He, Q., Feng, Y., & Mao, J. (2013a). Cloud-scale simulation study of Typhoon Hagupit (2008) Part I: Microphysical processes of the inner core and three-dimensional structure of the latent heat budget. *Atmospheric Research*, *120-121*, 170–180. https://doi.org/10.1016/j.atmosres.2012.08.015

Li, J., Wang, G., Lin, W., He, Q., Feng, Y., & Mao, J. (2013b). Cloud-scale simulation study of Typhoon Hagupit (2008) Part II: Impact of cloud microphysical latent heat processes on typhoon intensity. *Atmospheric Research*, *120–121*, 202–215. https://doi.org/10.1016/j.atmosres.2012.08.018

Li, X., & Pu, Z. (2008). Sensitivity of numerical simulation of early rapid intensification of Hurricane Emily (2005) to cloud microphysical and planetary boundary layer parameterizations. *Monthly Weather Review*, *136*(12), 4819–4838. https://doi.org/10.1175/2008MWR2366.1

Li, Y., Zipser, E. J., Krueger, S. K., & Zulauf, M. A. (2008). Cloud-resolving modeling of deep convection during KWAJEX. Part I: Comparison to TRMM satellite and ground-based radar observations. *Monthly Weather Review*, *136*(7), 2699–2712. https://doi.org/10.1175/2007MWR2258.1

Lin, Y., Farley, R. D., & Orville, H. D. (1983). Bulk parameterization of the snow field in a cloud model. *Journal of Applied Meteorology and Climatology*, *22*(6), 1065–1092. https://doi.org/10.1175/1520-0450(1983)022<1065:BPOTSF>2.0.CO;2

Lord, S. J., Willoughby, H. E., & Piotrowicz, J. M. (1984). Role of a parameterized ice-phase microphysics in an axisymmetric, nonhydrostatic tropical cyclone model. *Journal of the Atmospheric Sciences*, *41*(19), 2836–2848. https://doi.org/10.1175/1520-0469(1984)041<2836:ROAPIP>2.0.CO;2

Lynn, B. H., Khain, A. P., Bao, J. W., Michelson, S. A., Yuan, T., Kelman, G., et al. (2016). The sensitivity of Hurricane Irene to aerosols and ocean coupling: Simulations with WRF spectral bin microphysics. *Journal of the Atmospheric Sciences*, *73*(2), 467–486. https://doi.org/10.1175/JAS-D-14-0150.1

Masson, V., Le Moigne, P., Martin, E., Faroux, S., Alias, A., Alkama, R., et al. (2013). The SURFEXv7.2 externalized platform for the simulation of Earth surface variables and fluxes. *Geoscientific Model Development*, *6*, 929–960. https://doi.org/10.5194/gmd-6-929-2013

McFarquhar, G. M., & Black, R. A. (2004). Observations of particle size and phase in tropical cyclones: Implications for mesoscale modeling of microphysical processes. *Journal of the Atmospheric Sciences*, *61*(4), 422–439. https://doi.org/10.1175/1520-0469(2004)061<0422:OOPSAP>2.0.CO;2

McFarquhar, G. M., Zhang, H., Heymsfield, G., Halverson, J. B., Hood, R., Dudhia, J., & Marks, F. (2006). Factors affecting the evolution of Hurricane Erin (2001) and the distributions of hydrometeors: Role of microphysical processes. *Journal of the Atmospheric Sciences*, *63*(1), 127–150. https://doi.org/10.1175/JAS3590.1

Mei, W., Pasquero, C., & Primeau, F. (2012). The effect of translation speed upon the intensity of tropical cyclones over the tropical ocean. *Geophysical Research Letters*, *39*, L07801. https://doi.org/10.1029/2011GL050765

Milbrandt, J. A., & Yau, M. K. (2005). A multimoment bulk microphysics parameterization. Part II: A Proposed Three-Moment Closure and Scheme Description. *Journal of the Atmospheric Sciences*, *62*(9), 3065–3081. https://doi.org/10.1175/JAS3535.1

Mlawer, E. J., Taubman, S. J., Brown, P. D., Iacono, M. J., & Clough, S. A. (1997). Radiative transfer for inhomogeneous atmospheres: RRTM, a validated correlated-k model for the longwave. *Journal of Geophysical Research*, *102*(D14), 16,663–16,682. https://doi.org/10.1029/97JD00237

Mohktari, M., Gomes, L., Tulet, P., & Rezoug, T. (2012). Importance of the surface size distribution of erodible material: An improvement of the dust entrainment and deposition (DEAD) model. *Geoscientific Model Development*, *5*(3), 581–598. https://doi.org/10.5194/gmd-5-581-2012

Monahan, E. C., Spiel, D. E., & Davidson, K. L. (1986). In E. C. Monahan & G. MacNiocaill (Eds.), *A model of marine aerosol generation via whitecaps and wave disruption, oceanic whitecaps and their role in air-sea exchange processes* (pp. 167–174). Dordrecht, Netherlands: Reidel.

Morcrette, J.-J., Boucher, O., Jones, L., Salmond, D., Bechtold, P., Beljaars, A., et al. (2009). Aerosol analysis and forecast in the European Centre for Medium-Range Weather Forecasts Integrated Forecast System: Forward modeling. *Journal of Geophysical Research*, *114*, D06206. https://doi.org/10.1029/2008JD011235

O'Dowd, C. D., Lowe, J., Smith, M. H., & Kaye, A. D. (1999). The relative importance of non-sea-salt sulphate and sea-salt aerosol to the marine cloud condensation nuclei population: An improved multi-component aerosol-droplet parameterization. *Quarterly Journal of the Royal Meteorological Society*, *125*(556), 1295–1313. https://doi.org/10.1002/qj.1999.49712555610

Ovadnevaite, J., Manders, A., de Leeuw, G., Ceburnis, D., Monahan, C., Partanen, A.-I., et al. (2014). A sea spray aerosol flux parameterization encapsulating wave state. *Atmospheric Chemistry and Physics*, *14*(4), 1837–1852. https://doi.org/10.5194/acp-14-1837-2014

Phillips, V. T., DeMott, P. J., & Andronache, C. (2008). An empirical parameterization of heterogeneous ice nucleation for multiple chemical species of aerosol. *Journal of the Atmospheric Sciences*, *65*(9), 2757–2783. https://doi.org/10.1175/2007JAS2546.1

Phillips, V. T., Demott, P. J., Andronache, C., Pratt, K. A., Prather, K. A., Subramanian, R., & Twohy, C. (2013). Improvements to an empirical parameterization of heterogeneous ice nucleation and its comparison with observations. *Journal of the Atmospheric Sciences*, *70*(2), 378–409. https://doi.org/10.1175/JAS-D-12-080.1

Pianezze, J., Barthe, C., Bielli, S., Tulet, P., Jullien, S., Cambon, G., et al. (2018). A new coupled ocean-waves-atmosphere model designed for tropical storm studies: Example of tropical cyclone Bejisa (2013–2014) in the South-West Indian Ocean. *Journal of Advances in Modeling Earth Systems*, *10*(3), 801–825. https://doi.org/10.1002/2017MS001177

Pinty, J.-P., & Jabouille, P. (1998). A mixed-phase cloud parameterization for use in mesoscale non-hydrostatic model: Simulations of a squall line and of orographic precipitations, proceedings of conference on cloud physics, Everett, WA, USA. *American Meteorological Society*, 217–220.

Pruppacher, H. R. (1995). A new look at homogeneous ice nucleation in supercooled water drops. *Journal of the Atmospheric Sciences*, *52*(11), 1924–1933. https://doi.org/10.1175/1520-0469(1995)052<1924:ANLAHI>2.0.CO;2

Rosenfeld, D., Woodley, W. L., Khain, A., Cotton, W. R., Carrió, G., Ginis, I., & Golden, J. H. (2012). Aerosol effects on microstructure and intensity of tropical cyclones. *Bulletin of the American Meteorological Society*, *93*(7), 987–1001. https://doi.org/10.1175/BAMS-D-11-00147.1

Rutledge, S. A., & Hobbs, P. (1983). The mesoscale and microscale structure and organization of clouds and precipitation in midlatitude cyclones. VIII: A model for the "seeder-feeder" process in warm-frontal rainbands. *Journal of the Atmospheric Sciences*, *40*(5), 1185–1206. https://doi.org/10.1175/1520-0469(1983)040<1185:TMAMSA>2.0.CO;2

Saleeby, S. M., & Cotton, W. R. (2008). A binned approach to cloud-droplet riming implemented in a bulk microphysics model. *Journal of Applied Meteorology and Climatology*, *47*(2), 694–703. https://doi.org/10.1175/2007JAMC1664.1

Shpund, J., Pinsky, M., & Khain, A. (2011). Microphysical structure of the marine boundary layer under strong wind and spray formation as seen from simulations using a 2D explicit microphysical model. Part I: The Impact of Large Eddies. *Journal of the Atmospheric Sciences*, *68*(10), 2366–2384. https://doi.org/10.1175/2011JAS3652.1

Shpund, J., Zhang, J. A., Pinsky, M., & Khain, A. (2012). Microphysical structure of the marine atmospheric mixed layer under strong wind and sea spray formation as seen from a 2D explicit microphysical model. Part II: The Role of Sea Spray. *Journal of the Atmospheric Sciences*, *69*(12), 3501–3514. https://doi.org/10.1175/JAS-D-11-0281.1

Shpund, J., Zhang, J. A., Pinsky, M., & Khain, A. (2014). Microphysical structure of the marine boundary layer under strong wind and sea spray formation as seen from a 2D explicit microphysical model. Part III: Parameterization of height-dependent droplet size distribution. *Journal of the Atmospheric Sciences*, *71*(6), 1914–1934. https://doi.org/10.1175/JAS-D-12-0201.1

Slinn, W. G. N. (1983). *Atmospheric sciences and power production 1979, chap. 11*. Washington, DC: Precipitation Scavenging, U.S. Department of Energy.

Stephens, G. L., Vane, D. G., Boain, R. J., Mace, G. G., Sassen, K., Wang, Z., et al. (2002). The Cloudsat mission and the A-train. *Bulletin of the American Meteorological Society*, *83*(12), 1771–1790. https://doi.org/10.1175/BAMS-83-12-1771

Thompson, G., Field, P. R., Rasmussen, R. M., & Hall, W. D. (2008). Explicit forecasts of winter precipitation using an improved bulk microphysics scheme. Part II: Implementation of a new snow parameterization. *Monthly Weather Review*, *136*(12), 5095–5115. https://doi.org/10.1175/2008MWR2387.1

Tulet, P., Crahan-Kaku, K., Leriche, M., & Aouizerats, B. (2010). Mixing of dust aerosols into a mesoscale convective system. Generation, filtering and possible feedbacks on ice anvils. *Atmospheric Research*, *96*(2-3), 302–314. https://doi.org/10.1016/j.atmosres.2009.09.011

Tulet, P., Crassier, V., Cousin, F., Shure, K., & Rosset, R. (2005). ORILAM, a three moment lognormal aerosol scheme for mesoscale atmospheric model. On-line coupling into the MesoNH-C model and validation on the ESCOMPTE campaign. *Journal of Geophysical Research*, *110*, D18201. https://doi.org/10.1029/2004JD005716

Tulet, P., Mallet, M., Pont, V., Pelon, J., & Boone, A. (2008). The 7–13 March, 2006, dust storm over West Africa: Generation, transport and vertical stratification. *Journal of Geophysical Research*, *113*, D00C08. https://doi.org/10.1029/2008JD009871

Twomey, S. (1959). The nuclei of natural cloud formation part II: The supersaturation in natural clouds and the variation of cloud droplet concentration. *Geofisica Pura e Applicata*, *43*(1), 243–249. https://doi.org/10.1007/BF01993560

Twomey, S. (1977). The influence of pollution on the shortwave albedo of clouds. *Journal of the Atmospheric Sciences*, *34*(7), 1149–1152. https://doi.org/10.1175/1520-0469(1977)034<1149:TIOPOT>2.0.CO;2

Van den Heever, S. C., Carrió, G. G., Cotton, W. R., DeMott, P. J., & Prenni, A. J. (2006). Impacts of nucleating aerosol on Florida storms. Part I: Mesoscale simulations. *Journal of the Atmospheric Sciences*, *63*(7), 1752–1775. https://doi.org/10.1175/JAS3713.1

Van den Heever, S. C., & Cotton, W. R. (2007). Urban aerosol impacts on downwind convective storms. *Journal of Applied Meteorology and Climatology*, *46*(6), 828–850. https://doi.org/10.1175/JAM2492.1

Veron, F. (2015). Ocean sprays. *Annual Review of Fluid Mechanics*, *47*(1), 507–538. https://doi.org/10.1146/annurev-fluid-010814-014651

Vié, B., & Pinty, J.-P. (2014). LIMA: A two-moment mixed-phase microphysical scheme driven by a multimodal population of cloud condensation and ice freezing nuclei. Proceedings of 14th Conference on Cloud Physics. Boston, MA: American Meteorological Society.

Vié, B., Pinty, J.-P., Berthet, S., & Leriche, M. (2016). LIMA (v1.0): A quasi two-moment microphysical scheme driven by a multimodal population of cloud condensation and ice freezing nuclei. *Geoscientific Model Development*, *9*(2), 567–586. https://doi.org/10.5194/gmd-9-567-2016

Voldoire, A., Decharme, B., Pianezze, J., Lebeaupin Brossier, C., Sevault, F., Seyfried, L., et al. (2017). The seamless and multi-model coupling between atmosphere, land, hydrology, ocean, waves and sea-ice models based on SURFEX surface model using OASIS3-MCT. *Geoscience Model Development Discussion*, *10*, 1–39. https://doi.org/10.5194/gmd-2017-91

Wang, Y. (2002). An explicit simulation of tropical cyclones with a triply nested movable mesh primitive equation model: TCM3. Part II: Model refinements and sensitivity to cloud microphysics parameterization. *Monthly Weather Review*, *130*(12), 3022–3036. https://doi.org/10.1175/1520-0493(2002)130<3022:AESOTC>2.0.CO;2

Wang, Y., Kepert, J. D., & Holland, G. J. (2001). The effect of sea spray evaporation on tropical cyclone boundary layer structure and intensity. *Monthly Weather Review*, *129*(10), 2481–2500. https://doi.org/10.1175/1520-0493(2001)129<2481:TEOSSE>2.0.CO;2

Wang, Y., Lee, K.-H., Lin, Y., Levy, M., & Zhang, R. (2014). Distinct effects of anthropogenic aerosols on tropical cyclones. *Nature Climate Change*, *4*(5), 368–373. https://doi.org/10.1038/nclimate2144

Willoughby, H. E., Marks, F. D., & Feinberg, R. J. (1984). Stationary and moving convective bands in hurricanes. *Journal of the Atmospheric Sciences*, *41*(22), 3189–3211. https://doi.org/10.1175/1520-0469(1984)041<3189:SAMCBI>2.0.CO;2

Winker, D. M., Pelon, J., Coakley, J. A., Ackerman, S. A., Charlson, R. J., Colarco, P. R., et al. (2010). The CALIPSO mission. *Bulletin of the American Meteorological Society*, *91*(9), 1211–1230. https://doi.org/10.1175/2010BAMS3009.1

Winker, D. M., Pelon, J., & McCormick, M. P. (2003). The CALIPSO mission: Spaceborne lidar for observation of aerosols and clouds. In U. N. Singh, T. Itabe, & Z. Lui, (Eds.), *Lidar Remote Sensing for Industry and Environment Monitoring III, International Society for Optical Engineering (SPIE Proceedings)* (Vol. 4893, pp. 1–11).

Zender, C. S., Bian, H., & Newman, D. (2003). Mineral dust entrainment and deposition (DEAD) model: Description and 1990s dust climatology. *Journal of Geophysical Research*, *108*(D14), 4416. https://doi.org/10.1029/2002JD002775

Zhang, H., McFarquhar, G. M., Saleeby, S. M., & Cotton, W. R. (2007). Impacts of Saharan dust as CCN on the evolution of an idealized tropical cyclone. *Geophysical Research Letters*, *34*, L14812. https://doi.org/10.1029/2007GL029876

Zhu, T., & Zhang, D. (2006). Numerical simulation of Hurricane Bonnie (1998). Part II: Sensitivity to varying cloud microphysical processes. *Journal of the Atmospheric Sciences*, *63*(1), 109–126. https://doi.org/10.1175/JAS3599.1